IEEE Access
Multidisciplinary ⋮ Rapid Review ⋮ Open Access Journal

Received April 14, 2020, accepted May 2, 2020, date of publication May 6, 2020, date of current version May 20, 2020.

Digital Object Identifier 10.1109/ACCESS.2020.2992681

Parameters Identification and Application of Equivalent Circuit at Low Frequency of Oil-Paper Insulation in Transformer

YIMING XIE, (Student Member, IEEE), AND JIANGJUN RUAN, (Member, IEEE)
School of Electrical Engineering and Automation, Wuhan University, Wuhan 430072, China

Corresponding author: Yiming Xie (xieyiming@whu.edu.cn)

This work was funded by the China Scholarship Council, the funding number is 201906270135.

ABSTRACT The low frequency section of frequency domain spectroscopy (FDS) of oil-paper insulation system can effectively reflect the ageing state and moisture of the oil-immersed paper. Meanwhile, steady-state insulation resistance is the one of indexes for the condition of transformer. In actual measurement, these two both are time-consuming and poor accessibility, thereby restraining their field applications. Aim at this problem, this paper analyses the polarization process of the oil-paper insulation in transformer, and adopts a low frequency equivalent circuit model for the oil-paper insulation to characterize the polarization process at low frequency. The simulated annealing particle swarm optimization (SAPSO) algorithm is proposed to identify the parameters in equivalent circuit, which are affected by change of insulation state. Compared with the experimental results, the errors of the steady-state insulation resistance and the tan δ below 10^{-3} Hz, which are calculated by the identified parameters, are less than 2.5%. This method can avoid the influence from external environment and reduce the measurement time. The time and frequency domain parameters calculated can provide reference for the ageing assessment of oil-immersed paper.

INDEX TERMS Oil-paper insulation equivalent circuit, interfacial polarization, simulated annealing particle swarm optimization, steady-state insulation resistance, frequency domain spectroscopy.

I. INTRODUCTION

Oil immersed power transformer is one of the most widely used equipment in power system. Because the oil can be filtered or replaced, the insulation state of oil-immersed paper determines the transformer life [1]. It is difficulty to directly detect the insulation state of the oil-immersed paper inside the transformer without dismantling the shell. The process of sampling is poor accessibility to operate [2]. In recent years, based on dielectric response, the non-destructive evaluation method of insulation state of transformer, such as recovery voltage method (RVM), polarization and depolarization current (PDC), frequency domain spectroscopy (FDS), has gradually become the research focus [3]–[6]. According to [7], [8], tan δ at low frequency is sensitive to the ageing state and moisture of oil-immersed paper. In [9], [10], the final magnitudes of polarization current (Leakage current, corresponding to steady-state insulation resistance), reflecting oil-immersed paper state, have been influenced by ageing and moisture. All of them can provide rich insulation information for technicians. However, the measurement time of tan δ at low frequency and the polarization current are too long. For example, measured time of the tan δ at 10^{-4} Hz and polarization current at 10^4 s are about 5 hours. Meanwhile, the measured values are easily affected by the environment, which is not conducive to the field application.

Establishing oil-paper insulation equivalent circuit is an effective and simple way to calculate low-frequency tan δ and steady-state insulation resistance, then can assess the insulation state. The deterioration of insulation state can alter the dielectric characteristics [11], which lead to the change of parameters in equivalent circuit. Hence, solving these parameters can obtain the characteristic parameters related to the insulation state. Comparing the changes of

The associate editor coordinating the review of this manuscript and approving it for publication was Huiling Chen.

This work is licensed under a Creative Commons Attribution 4.0 License. For more information, see https://creativecommons.org/licenses/by/4.0/

these parameters can also reflect the insulation status of the transformer to a certain extent [12]. References [12]–[14] used the extend Debye model to model the PDC or RVM data by the least square method. References [15], [16] used Maxwell or Debye model to simulate RVM curves, which gain the good results. These researches are fitting by complete PDC or RVM experimental data curves as input. There are few researches on how to quickly obtain the final magnitudes of PDC or low-frequency FDS.

How to establish appropriate low-frequency equivalent circuit is the key. Previous studies [12]–[14], [16] were based on extended Debye model. However, the oil-paper insulation consists of two dielectrics. Besides the dipole polarization produced by dipole orientation in each dielectric, the oil-paper insulation will form a complex interfacial polarization due to accumulation of charge at interface. The process of interfacial polarization is usually determined by the conductivity and relative permittivity of the two kinds of dielectric. The *RC* series branch in Debye model cannot truly reflect the complex interfacial polarization phenomenon. Identification method is also important to solve the parameters in circuit, reference [14] used iterative method to solve the parameters, which is affected by initial parameters easily. To avoid this, intelligent algorithms are a better choice.

In this paper, the Maxwell model is used to characterize the polarization process of oil-paper insulation at low frequency section, in which the interfacial polarization plays a major role and the dipole polarization of a single dielectric has little impact [17]. Insulation resistance formula is used to establish the mathematical model for parameters identification. The parameters can be identified by inputting the data from the 30 min insulation resistance curve. For identification method, SAPSO is used to overcome the shortcomings of PSO that easily fall into local optimum. Finally, the identified parameters are applied to the calculation of the steady-state insulation resistance values and tan δs whose frequency below the 10^{-3} Hz, which greatly reduces the measurement time of steady-state insulation resistance and the tan δ at low frequency, and provides a reference for the judgement of the insulation state of the oil-immersed paper.

II. ANALYSIS ON DIELECTRIC RESPONSE OF OIL-PAPER INSULATION AT LOW FREQUENCY

A. POLARIZATION CHARACTERISTICS OF OIL-PAPER INSULATION AT LOW FREQUENCY

Due to the existence of dielectric conductivity and the dielectric polarization under the action of AC voltage, the energy loss produced in the dielectric is called the dielectric loss. The dielectric loss in single dielectric is composed of conductance loss, displacement polarization loss and dipole polarization loss. The displacement polarization is extremely fast and thus effective up to infra-red frequencies or optical frequencies, which can be neglected, while the duration of the dipole polarization is longer, which occurs in mid-high frequencies [5], [18]. When the dielectric is a composite material, such as oil-paper insulation, there will be interfacial polarization, whose process active in the power frequency range and below and produce energy loss [5].

Due to the duration of dipole polarization is less than period of electric field at low frequency, the polarization can be fully established without hysteresis, and the contribution of dipole polarization loss to total loss can be neglected [17]–[19]. The oil-paper insulation is a composite material. The interfacial polarization always occurs in middle and low frequency section and even at DC voltage (within hours after applying DC voltage) due to longer relaxation time. Therefore, it can conclude that the dielectric loss of oil-paper insulation at low frequency and DC voltage is mainly composed of conductance loss and interfacial polarization loss. To reduce the influence of applied AC voltage and geometric structure, the dielectric loss factor tan δ is introduced to characterize the dielectric loss.

To consider the influence of interfacial polarization, the equivalent circuit of Maxwell model is established as shown in Fig 1. The resistance and capacitance of paper and oil are R_1, C_1, and R_2, C_2 respectively in Fig 1.

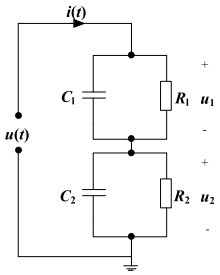

FIGURE 1. Maxwell model.

B. EQUIVALENT MODEL OF OIL-PAPER INSULATION

The oil-immersed paper is a weak link in the insulation of the transformer, and its insulation state determines the operation life of transformer [1]. The insulation state of oil-immersed paper has a strong correlation with the final part of polarization current and low-frequency tan δ. Therefore, obtaining steady-state insulation resistance and low-frequency tan δ through accurate calculation are significant to the condition assessment of oil-paper insulation. Establishing the equivalent model is good way to realize it.

The extended Debye model of oil-paper insulation is shown in Fig 2, where R_g is the steady-state insulation

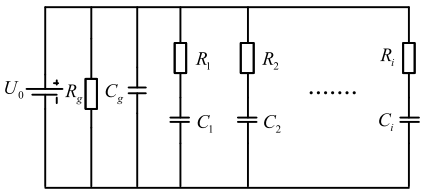

FIGURE 2. The extended Debye model of oil-paper insulation.

resistance, C_g is the geometric capacitance. R_i and C_i are the resistance and capacitance in the ith branch. The different time constants, given by $\tau_i = R_i C_i$, are used to represent the different processes of polarization response in the extended Debye model, which does not consider the geometric structure of the oil-paper insulation.

The oil-paper insulation is a kind of composite insulating dielectric. The RC series branches in Debye model cannot reflect the interfacial polarization between different materials by insulation structure. From the above analysis in subsection A, the loss of oil-paper insulation at low frequency is mainly composed of conductance loss and interfacial polarization loss. To characterize the interfacial polarization, the Maxwell model is used into the equivalent circuit of oil-paper insulation, shown in the Fig 3, where the conductance loss is caused by the resistance existing in the circuit, and the parallel structure of two dielectrics can reflect the interfacial polarization process.

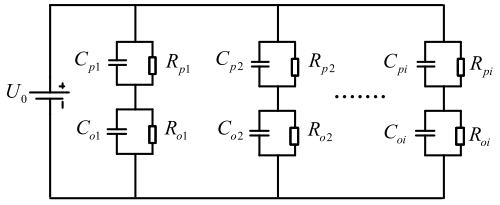

FIGURE 3. The equivalent circuit of oil-paper insulation.

In Fig 3, the subscript p and o denote paper and oil respectively, and i indicates the number of branch. The R_{pi}, R_{oi} and C_{pi}, C_{oi} represent the resistance and capacitance of transformer paper and oil in ith branch.

III. MATHEMATICAL MODEL AND PARAMETERS IDENTIFICATION OF EQUIVALENT CIRCUIT

A. OPTIMAL OBJECTIVE FUNCTION

The effective identification of the parameters in the equivalent circuit is of great significance to the evaluation of the insulation state. Due to the initial derivative of recovery voltage and the recovery voltage correspond with the insulation sate of transformer, the previous researches focused on modeling the dielectric response of transformer insulation with RVM [14]–[16]. Although they can be both used to identify the parameters of the equivalent circuit, the laplace transform of recovery voltage is so difficulty to deduce that it leads to enormous calculation when the number of branches is increased [14]. Meanwhile, the RVM measurement signal is easily disturbed by environment. Compared to recovery voltage method, insulation resistance measurement is more widely used monitoring method in field measurement, meanwhile, it contains rich information and is less interference by other signal. Therefore, this paper uses the mathematical model of insulation resistance to build the optimal objective function to identify the parameters.

The DC voltage of u_0 is loaded on the transformer port, take the equivalent circuit in Fig 3 as an example. Before the loading, $u_{cpi}(0_-) = u_{coi}(0_-) = 0$. After loading, the voltage $u_{cpi}(t)$, $u_{coi}(t)$ at capacitance of paper and oil satisfy the equation as follows.

$$u_{cpi}(0_+) + u_{coi}(0_+) = u_0 \tag{1}$$

According to the charge conservation:

$$C_{pi}u_{cpi}(0_+) - C_{oi}u_{coi}(0_+) = C_{pi}u_{cpi}(0_-) - C_{oi}u_{coi}(0_-) \tag{2}$$

The $u_{cpi}(0_+)$ can be deduced:

$$u_{cpi}(0_+) = \frac{C_{oi}}{C_{pi} + C_{oi}} u_0 \tag{3}$$

The time constant of ith branch is:

$$\tau_i = \frac{R_{pi}R_{oi}}{R_{pi} + R_{oi}}(C_{pi} + C_{oi}) \tag{4}$$

The $u_{cpi}(t)$ can be deduced:

$$u_{cpi}(t) = \frac{R_{pi}}{R_{pi}+R_{oi}} u_0 - \frac{R_{pi}C_{pi} - R_{oi}C_{oi}}{(R_{pi}+R_{oi})(C_{pi}+C_{oi})} u_0 e^{-t/\tau_i} \tag{5}$$

The current $I_i(t)$ flows through the ith branch is:

$$\begin{aligned} I_i(t) &= \frac{u_{cpi}(t)}{R_{pi}} + C_{pi}\frac{u_{cpi}(t)}{dt} \\ &= \left[\frac{R_{pi}C_{pi}^2 + R_{oi}C_{oi}^2}{R_{pi}R_{oi}(C_{pi} + C_{oi})^2} - \frac{1}{R_{pi} + R_{oi}}\right] u e^{-\frac{t}{\tau}} + \frac{u}{R_{pi}+R_{oi}} \end{aligned} \tag{6}$$

The insulation resistance of equivalent circuit can be expressed as:

$$R(t) = u_0/[I_1(t) + I_2(t) + \cdots I_i(t) + \cdots I_n(t)] \tag{7}$$

In (1)∼(7), u_0, t, $R(t)$ can be obtained by on-site measurement. The unknown parameters are represent as $\boldsymbol{x_i} = (R_{pi}, R_{ci}, C_{pi}, C_{oi})$, $i = 1, 2 \ldots n$. n is the number of branches. m is set as the number of unknown parameters. Obviously, $m = 4n$. It is necessary to adopt m equations to solve m unknowns to ensure unique solutions. In this paper, m values of insulation resistance and corresponding charging time t are selected through experimental curve, and the m equation is:

$$\begin{cases} R(t_1) = u_0/[I_1(t_1) + I_2(t_1) + \cdots I_n(t_1)] \\ \cdots \\ R(t_m) = u_0/[I_1(t_m) + I_2(t_m) + \cdots I_n(t_m)] \end{cases} \tag{8}$$

The problem of solving (8) is transformed into a problem of mathematical optimization. The optimal objective function can be established by the least square method as (9). When $F(\boldsymbol{x}) = 0$, the parameters can be identified.

$$F(\boldsymbol{x}) = \min\{[\frac{1}{m}\sum_{j=1}^{m}(\frac{R(t_j) - \frac{u_0}{I_1(t_j)+I_2(t_j)+\cdots I_i(t_j)}}{R(t_j)})]^2\} \tag{9}$$

where $R(t_j)$ represents the measured value of insulation resistance in charge time of t_j.

B. SIMULATED ANNEALING PARTICLE SWARM OPTIMIZATION

The methods of solving nonlinear equations mainly include the Newton method, continuation method, the steepest descent method and so on, where the Newton method is widely used. However, improper selection of initial values will lead to divergence of solutions in the Newton method [20]. In this paper, the initial value ranges of resistance and capacitance parameters of each branch are not sure. Therefore, it is difficulty to accurately solve the parameters in equivalent circuit by the numerical iterative method. Therefore, intelligent optimized algorithms are a better choice.

Particle swarm optimization (PSO) is an evolutionary algorithm based on swarm intelligence, which is fast in convergence speed. The whole group shows a strong ability of optimization through the information exchange between each particle [21]. Nevertheless, the complex functions to be optimized in the actual engineering have the characteristics of nonlinear, discrete and multi-peak, which will lead to the aggregation of particle swarm in the local extremum. Hence, it is important to improve the ability of global search in PSO, and guarantee the quality of the solution.

The simulated annealing (SA) algorithm origins in the physical annealing process of heating up a solid to a high temperature followed by cooling slowly. In the process of searching the solution space, SA has the possibility to accept worse solutions in a controlled manner for escaping from local minima [22]. The probability of acceptance decreases gradually with the decrease of temperature. In short, SA can avoid the local minimum by giving a probability jump to the search process, which is time-varying and eventually tends to 0.

Therefore, the combination of PSO and SA, namely, the simulated annealing particle swarm optimization (SAPSO) makes full use of the advantages of the fast convergence ability of PSO and the local extreme jump ability of SA [23]. It can effectively avoid the local extremum in the search process and find true solutions quickly. The steps of SAPSO are as follows.

1) Randomly initialize the location vector $\boldsymbol{x}_i$ and speed vector $\boldsymbol{v}_i$ of particle swarm, $i = 1, 2, \ldots N$, where, N is the particle population. Determine learning factors c_1, c_2, compressibility factor k in (10), maximum iterative number t;

$$k = \frac{2}{\left|2-(c_1+c_2)-\sqrt{(c_1+c_2)^2-4(c_1+c_2)}\right|} \tag{10}$$

2) Calculate the fitness values of the initial particle swarm $F(\boldsymbol{x}_i)$. The initial position vector $\boldsymbol{x}_i$ is set as the initial local optimum location $\boldsymbol{p}_i$;
3) Compare the fitness values of each particle, set the location corresponding to the minimum fitness value of the particle swarm as the global optimal location $\boldsymbol{p}_{ng}$, iteration start;
4) Set the initial temperature as $T = F(\boldsymbol{p}_g)/\mathrm{In}(p_r)$, p_r is the initial acceptance probability;
5) Set the appropriate value as $TF(\boldsymbol{p}_i)$ at the current temperature, the $TF(\boldsymbol{p}_i)$ is as follows:

$$TF(\boldsymbol{p}_i) = \frac{e^{-(F(\boldsymbol{p}_i)-F(\boldsymbol{p}_g))/T}}{\sum_{i=1}^{N} e^{-(F(\boldsymbol{p}_i)-F(\boldsymbol{p}_g))/T}} \tag{11}$$

6) Accept the new global optimal location $\boldsymbol{p}_g$ by adopting the roulette strategy, that is to say, if $TF(\boldsymbol{p}_i) > rand$, the new global optimal location is accepted, otherwise the original global optimal position is retained. Where, *rand* means the random number between 0 and 1;
7) Update the speed and position of the next generation particle according to (12).

$$\begin{cases} v_{id}(t+1) \\ = k[v_{id}(t)+c_1r_1(p_{id}-x_{id}(t))+c_2r_2(p_{gd}-x_{id}(t))] \\ x_{id}(t+1) \\ = x_{id}(t)+v_{id}(t), \quad i=1, 2, \ldots N, \ d=1, 2, \ldots, m \end{cases} \tag{12}$$

where d represents the dimension of each particle.
8) Calculate the fitness value of each updated particle and update $\boldsymbol{p}_i$ and $\boldsymbol{p}_g$;
9) Execute the anneal instruction, $T(t) = \lambda T(t+1)$, where, λ is annealing speed;
10) If the $\boldsymbol{x}_i$ satisfies the condition of $F(\boldsymbol{x}_i) = 0$, the searching is stop, otherwise, go back to step (3) to continue searching.

The flow chart of SAPSO is as shown in Fig 4.

C. CALCULATION OF FDS

The AC voltage $\dot{U}_0$ is applied to the port of the equivalent circuit in Fig 3, the current of each branch can be expressed as:

$$I_i = \frac{U_0}{\frac{R_{pi}}{1+j\omega R_{pi}C_{pi}} + \frac{R_{oi}}{1+j\omega R_{oi}C_{oi}}}, \quad i = 1, 2 \cdots n \tag{13}$$

The tanδ of the equivalent circuit of oil-paper insulation can be expressed as:

$$\tan\delta = \frac{real(I_1 + I_2 + \cdots I_i)}{imag(I_1 + I_2 + \cdots I_i)} \tag{14}$$

where *real* and *imag* represent the real part and imaginary part, respectively.

The FDS is obtained by substituting the identified parameters and ω into (13) and (14).

IV. VERIFICATION OF EXPERIMENT

According to exist of interfacial polarization, the measured time of steady-state insulation resistance may last for several hours. For saving measured time and ensure the accuracy of identified parameter, this paper chose the data in 30 min insulation resistance measured curve to identify the parameters in equivalent circuit. Then, the parameters identified by SAPSO are used to calculate the tan δ below 10^{-3} Hz.

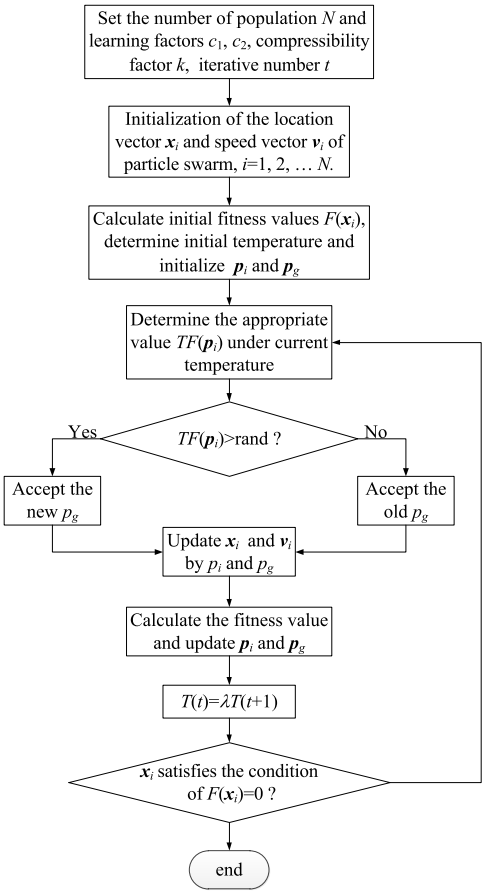

FIGURE 4. The flow chart of SAPSO.

TABLE 1. The setting of test connection.

Number of wiring mode	High voltage end of device (+)	Measured end of device (E)	Shielded end of device (G)
1	High voltage winding terminal	Low voltage winding terminal, shell	Copper wire of porcelain bushing
2	Low voltage winding terminal	High voltage winding terminal, shell	Copper wire of porcelain bushing

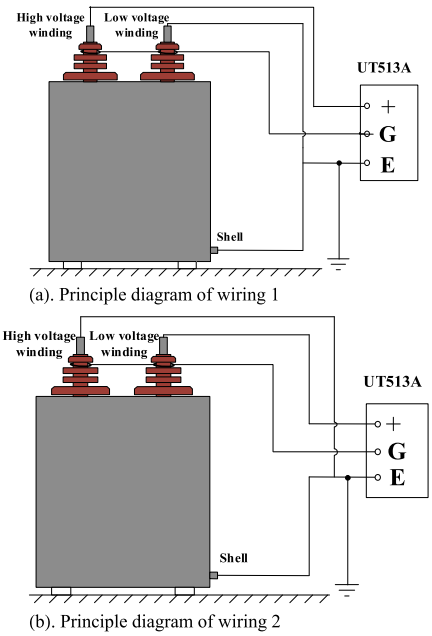

FIGURE 5. The schematic diagram of wiring.

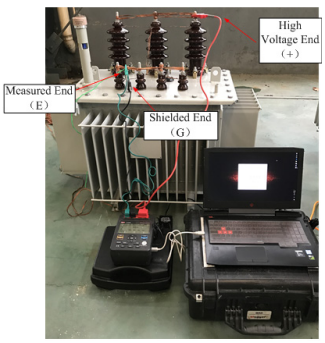

FIGURE 6. The physical map of wiring 1.

The test object is a new 200 kVA oil immersed transformer. Insulation resistance is measured by insulation resistance instrument UT513A, and the measured voltage and time is 5000V and 2h, measured curve is recorded every 1 s in real-time by computer. The IDAX300 produced by Megger company is used to measure the FDS of oil-paper insulation, and the measured voltage is 200V. The measured frequency range is 10^{-4} ~10^{3} Hz. The ambient temperature is 9~12 °C. For avoiding the interference of surface current, the copper wire on the porcelain bushing is connected with the shielding end (G) of the measuring device. The setting of test connection is shown as Table 1. The wiring principle diagrams are shown in Fig 5. Physical map of wiring mode 1 is shown as Fig 6. Different wiring modes correspond to different oil-paper insulation measured circuit.

The data in the 30 min insulation resistance curve, selected by the uniformly-spaced method (sampling step is 90s), are substituted into (9), and SAPSO is used to find the optimal solution. In this paper, to ensure the accuracy of parameter identification and avoid adding unnecessary parameters, the number of branches is set to 5, namely, there are 20 unknowns. The range of capacitance is set as [10^{-13}F,10^{-7}F], and the range of resistance is set as [$10^{7}\Omega$,$10^{13}\Omega$]. The number of iteration t is set as 1500 steps to control the computational efficiency. The number of particle $N = 40$. To ensure global searching ability of the algorithm, the learning factor $c_1 = 2.8$, $c_2 = 1.3$ [23]. In the part of SA, the initial temperature has a great influence on the global searching ability of the algorithm. Slower cooling process can improve the global search ability and increase the searching time, the annealing speed $\lambda = 0.99$. For ensuring the diversification of initial particle swarm, the initial acceptance probability p_r is 0.2.

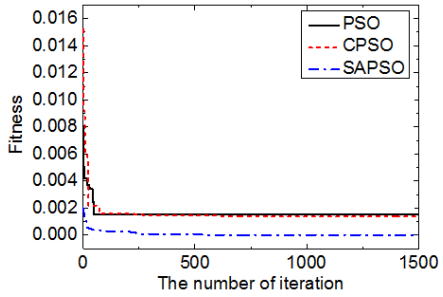

FIGURE 7. The fitness comparison of SAPSO and other PSO.

TABLE 2. Parameter identification results of wiring mode 1 and 2.

wiring mode 1				
Number of branch	Resistance (GΩ)		Capacitance (PF)	
1	R_{P1}	589.04	C_{P1}	4660.8
	R_{O1}	47.98	C_{O1}	264.60
2	R_{P2}	518.96	C_{P2}	21859
	R_{O2}	83.54	C_{O2}	2586.3
3	R_{P3}	296.88	C_{P3}	3291.3
	R_{O3}	9.65	C_{O3}	92.27
4	R_{P4}	294.57	C_{P4}	10987
	R_{O4}	808.98	C_{O4}	10.99
5	R_{P5}	3.30	C_{P5}	16.02
	R_{O5}	734.75	C_{O5}	93.43
wiring mode 2				
Number of branch	Resistance (GΩ)		Capacitance (PF)	
1	R_{P1}	8762.81	C_{P1}	177.76
	R_{O1}	100	C_{O1}	22935.17
2	R_{P2}	9703.54	C_{P2}	15518.58
	R_{O2}	54.91	C_{O2}	14025.89
3	R_{P3}	6892.62	C_{P3}	7408.96
	R_{O3}	31.23	C_{O3}	795.64
4	R_{P4}	1000	C_{P4}	70.41
	R_{O4}	8748.45	C_{O4}	0.30
5	R_{P5}	147.75	C_{P5}	663.29
	R_{O5}	0.090	C_{O5}	1000

The fitness of SAPSO is compared with that of PSO and chaotic particle swarm optimization (CPSO) to show the convergence efficiency and search ability of these algorithms, as shown in Fig 7. It can be concluded that the global search ability of SAPSO is much better than that of PSO and CPSO.

The results of parameters identification under the wiring mode 1 and 2 are as Table 2.

To verify the correctness of the parameters, the steady-state insulation resistance and FDS corresponding to the wiring mode 1 and 2 are calculated by the identified parameters, and the results are compared with the actual measured results, as shown in Fig 8∼9.

From Fig 8(a) and 9(a), the calculated curves of insulation resistance are fitted well with the measured curves. It can be found in Fig 8(b) and 9(b) that the overall trend of the calculated and measured curves is similar. Below 10^{-3} Hz, the calculated curves fit well, while in the 10^{-3}Hz∼10^{3} Hz, the measured curves first increase and then decrease, and the

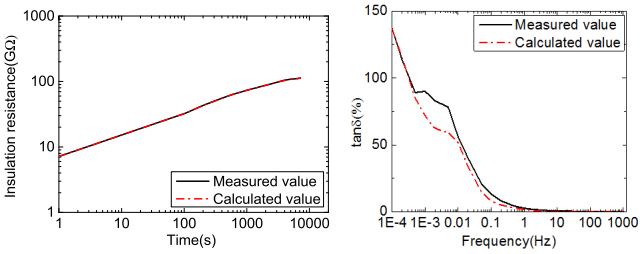

(a) steady state insulation resistance curves (b) FDS curves

FIGURE 8. The calculated curves of the steady state insulation resistance and FDS of the wiring 1.

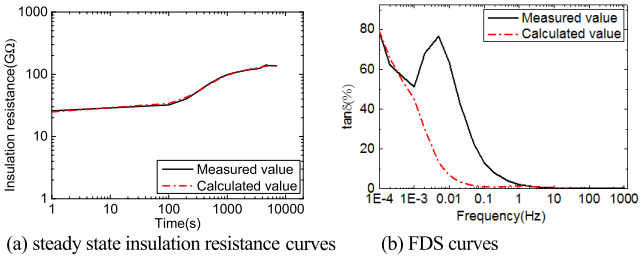

(a) steady state insulation resistance curves (b) FDS curves

FIGURE 9. The calculated curves of the steady state insulation resistance and FDS of the wiring 2.

calculated values are always lower than the measured values. This is because the equivalent circuit mentioned in section II can be suitable for the low frequency section, where the dipole polarization can be neglected. The details are discussed as follows.

1) Due to the $\omega \approx 0$ at low frequency, the dipole arrangement can keep up with the change of electric field, and no hysteresis in the process of dipole polarization, the dipole polarization loss can be neglected. Due to $\tan\delta \propto 1/\omega$[17-18], it is known that the $\tan\delta$ decreases with the increase of frequency.
2) When $\omega\tau \approx 1$, the cycle of the applied voltage is close to the time constant τ of dipole polarization, which makes the dipole polarization loss increase. Therefore, the measured curve will rise [18].
3) As the frequency increases, the voltage or electric field changes so faster that the polarization is not enough time to establish so that it decreases, meanwhile, conductance loss also decreases with the frequency increases, so the total loss gradually decreases [18]. To highlight the difference between the measured and calculated values in the mid-frequency, a linear axis is used in Fig. 8∼9. In these figures, the measured values and calculated values above 100 Hz seem to be the same, but in fact, the measured values are still higher than the calculated values in this frequency. The FDS measured by measurement contains conductance loss, dipole polarization loss and interfacial polarization loss, while the equivalent circuit based on Maxwell model in this paper only reflects the conductivity loss and the interfacial polarization loss at low frequency

TABLE 3. Error Analysis of The Steady-state Insulation Resistance and tan δ at $f < 5 \times 10^{-4}$ Hz.

The Number of Wiring Mode	e_{MSPE} of Steady-state Insulation Resistance (%)	e_{MSPE} of tan δ (%)
wiring mode 1	0.14	1.65
wiring mode 2	0.45	2.45

and neglects the polarization loss in the single dielectric. Therefore, in case of low frequency, the calculated curve can be consistent with the measured curve, while always lower than the measured values when $f > 10^{-3}$ Hz.

In this paper, the mean square percentage error (MSPE) is used as the index of error evaluation.

$$e_{MSPE} = \frac{1}{N}\sqrt{\sum_{i=1}^{N}(\frac{A_i - P_i}{A_i})^2} \tag{15}$$

where A_i is the ith measured value, P_i is the ith calculated value, N is the number of measured data.

The insulation resistance values, from 2000 s to steady state, are selected as the samples of insulation resistance, and the tan δ values at 5×10^{-4} Hz, 2×10^{-4} Hz and 1×10^{-4} Hz are selected as the tan δ samples at low frequency. The e_{MSPE} of steady-state insulation resistance and tan δ at low frequency are shown in Table 3. It is concluded that the e_{MSPE}s are all less than 2.5%, which proves correctness and reliability the equivalent circuit and identified method. It should be noticed that the method presented in this paper is not limited to obtain the tan δ of 0.1 mHz$\sim$1 mHz, but also to calculate more lower frequency data. The lower the frequency, the smaller the influence of dipole polarization on tan δ. Therefore, the lower the frequency, the more accurate the calculation results are. This is greatly beneficial to reduce the time of field measurement.

V. CONCLUSIONS

PDC and FDS are non-destructive assessment methods for transformer oil-paper insulation. The steady-state insulation resistance and tan δ at low frequency can reflect the insulation state of oil-immersed paper, but the measured time is too long and easily affected by environment signals. Based on Maxwell model, this paper studies the characteristics of dielectric polarization and establishes an equivalent circuit at low frequency of oil-paper insulation. Combining with the 30 min insulation resistance curve, the optimization algorithm is used to identify the circuit parameters effectively. The following conclusions can be obtained:

1) Based on the Maxwell model, the equivalent circuit can characterize the polarization process of the oil-paper insulation at low frequency;
2) Compared with PSO and CPSO, SAPSO has an improvement in global search ability and convergence speed. It can quickly identify the circuit parameters and improve the accuracy and efficiency of identified process;
3) The steady-state insulation resistance and tan δ below 10^{-3} Hz calculated by the identified parameters can coincide with the measured curves, and the maximal e_{MSPE}s are less than 2.5%. It proves the correctness and superiority of the equivalent circuit and identified method.

The method proposed in this paper can effectively shorten the field measurement time of tan δ below 10^{-3} Hz and the steady-state insulation resistance, which can provide effective data to assess the insulation state of transformer oil-paper insulation. In the follow-up study, to broaden frequency band, different equivalent models will be used to analyze the polarization types in different frequency bands, and a more comprehensive mathematical model will be established to obtain more effective data of FDS.

REFERENCES

[1] D. Martin, Y. Cui, C. Ekanayake, H. Ma, and T. Saha, "An updated model to determine the life remaining of transformer insulation," *IEEE Trans. Power Del.*, vol. 30, no. 1, pp. 395–402, Feb. 2015.

[2] M. Wang, A. J. Vandermaar, and K. D. Srivastava, "Review of condition assessment of power transformers in service," *IEEE Elect. Insul. Mag.*, vol. 18, no. 6, pp. 12–25, Nov. 2002.

[3] T. K. Saha and P. Purkait, "Investigation of polarization and depolarization current measurements for the assessment of oil-paper insulation of aged transformers," *IEEE Trans. Dielectr. Electr. Insul.*, vol. 11, no. 1, pp. 144–154, Feb. 2004.

[4] T. K. Saha and P. Purkait, "Investigation of an expert system for the condition assessment of transformer insulation based on dielectric response measurements," *IEEE Trans. Power Del.*, vol. 19, no. 3, pp. 1127–1134, Jul. 2004.

[5] W. S. Zaengl, "Dielectric spectroscopy in time and frequency domain for HV power equipment. I. Theoretical considerations," *IEEE Elect. Insul. Mag.*, vol. 19, no. 5, pp. 5–19, Sep. 2003.

[6] S. M. Gubanski, P. Boss, G. Csepes, V. Der Houbanessian, J. Filippini, and U. Gäfvert, "Dielectric response methods for diagnostics of power transformers," *IEEE Elect. Insul. Mag.*, vol. 19, no. 3, pp. 12–18, May/Jun. 2003.

[7] R. Liao, J. Hao, G. Chen, and L. Yang, "Quantitative analysis of ageing condition of oil-paper insulation by frequency domain spectroscopy," *IEEE Trans. Dielectr. Electr. Insul.*, vol. 19, no. 3, pp. 821–830, Jun. 2012.

[8] R. Jadav, C. Ekanayake, and T. Saha, "Understanding the impact of moisture and ageing of transformer insulation on frequency domain spectroscopy," *IEEE Trans. Dielectr. Electr. Insul.*, vol. 21, no. 1, pp. 369–379, Feb. 2014.

[9] I. Fofana, H. Hemmatjou, and M. Farzaneh, "Low temperature and moisture effects on polarization and depolarization currents of oil-paper insulation," *Electr. Power Syst. Res.*, vol. 80, no. 1, pp. 91–97, Jan. 2010.

[10] M. Koch and S. Tenbohlen, "Diagnostics of oil-paper insulations using relaxation currents," in *Proc. 14th Int. Symp. High Voltage Eng.*, Beijing, China, Aug. 2005, p. 507.

[11] M. G. Niasar, N. Taylor, H. Edin, and R. C. Kiiza, "Dielectric frequency response of oil-impregnated paper: The effect of partial discharges compared to other influences," *IEEE Trans. Dielectr. Electr. Insul.*, vol. 23, no. 3, pp. 1769–1777, Jun. 2016.

[12] T. K. Saha, P. Purkait, and F. Muller, "Deriving an equivalent circuit of transformers insulation for understanding the dielectric response measurements," *IEEE Trans. Power Del.*, vol. 20, no. 1, pp. 149–157, Jan. 2005.

[13] A. Bognar, G. Csepes, L. Kalocsai, and I. Kispal, "Spectrum of polarization phenomena of long time-constant as a diagnostic method of oil-paper insulating systems," in *Proc. 3rd Int. Conf. Properties Appl. Dielectr. Mater.*, vol. 2, 1991, pp. 723–726.

[14] P. R. S. Jota, S. M. Islam, and F. G. Jota, "Modeling the polarization spectrum in composite oil/paper insulation systems," *IEEE Trans. Dielectr. Electr. Insul.*, vol. 6, no. 2, pp. 145–151, Apr. 1999.

[15] R. Patsch and J. Menzel, "Ageing and degradation of power transformers-how to interpret return voltage measurements," in *Proc. Int. Symp. Electr. Insulating Mater.*, Sep. 2008, pp. 179–182.
[16] A. Szirmai and Z. A. Tamus, "Modelling of dielectric processes in oil-paper insulation for replacement of return voltage measurement," in *Proc. Conf. Diag. Electr. Eng. (Diagnostika)*, Sep. 2016, pp. 1–4.
[17] Y. Xie, J. Ruan, Y. Shi, S. Jin, Y. Tian, and L. Zhu, "Inversion detection method for resistivity of oil-immersed paper in transformer," *IEEE Trans. Power Del.*, vol. 34, no. 4, pp. 1757–1765, Aug. 2019.
[18] M. Dong, M. Ren, F. Wen, C. Zhang, J. Liu, C. Sumereder, and M. Muhr, "Explanation and analysis of oil-paper insulation based on frequency-domain dielectric spectroscopy," *IEEE Trans. Dielectr. Electr. Insul.*, vol. 22, no. 5, pp. 2684–2693, Oct. 2015.
[19] D. Linhjell, L. Lundgaard, and U. Gafvert, "Dielectric response of mineral oil impregnated cellulose and the impact of aging," *IEEE Trans. Dielectr. Electr. Insul.*, vol. 14, no. 1, pp. 156–169, Feb. 2007.
[20] K. Lange, "Newton's method and scoring," in *Numerical Analysis for Statisticians*. New York, NY, USA: Springer, 1999, pp. 130–142.
[21] J. Kennedy and R. Eberhart, "Particle swarm optimization," in *Proc. IEEE Int. Conf. Neural Netw.*, vol. 4, Dec. 1995, pp. 1942–1948.
[22] D. Bertsimas and J. Tsitsiklis, "Simulated annealing," *Statist. Sci.*, vol. 8, no. 1, pp. 10–15, 1993.
[23] J. Behnamian, M. Zandieh, and S. M. T. Fatemi Ghomi, "Due windows group scheduling using an effective hybrid optimization approach," *Int. J. Adv. Manuf. Technol.*, vol. 46, nos. 5–8, pp. 721–735, Jan. 2010.

YIMING XIE (Student Member, IEEE) was born in Anhui, China, in 1993. He is currently pursuing the Ph.D. degree in high-voltage and insulation technology from the School of Electrical Engineering and Automation, Wuhan University. His research interests include multiphysical field simulation, condition monitoring of electric equipment, high-voltage and insulation technology.

JIANGJUN RUAN (Member, IEEE) was born in Zhejiang, China, in 1968. He received the B.S. and Ph.D. degrees in electric machine engineering from the Huazhong Institute of Technology, Huazhong University of Science and Technology, Wuhan, China, in 1990 and 1995, respectively, and the Ph.D. degree from the Wuhan University of Hydraulic and Electric Engineering, Wuhan, China, in 1998. He is currently a Professor with Wuhan University, Wuhan. His research interests include electromagnetic field numerical simulation, high-voltage, and insulation technology.